Available online at www.sciencedirect.com
SCIENCE DIRECT®
Journal of Magnetic Resonance 171 (2004) 314–323
JMR Journal of Magnetic Resonance
www.elsevier.com/locate/jmr

# Cross polarization, radio frequency field homogeneity, and circuit balancing in high field solid state NMR probes

Eric K. Paulson, Rachel W. Martin, Kurt W. Zilm*

*Department of Chemistry, Yale University, P.O. Box 208107, New Haven, CT 06520-8107, United States*

Received 10 June 2004; revised 27 August 2004

**Abstract**

Homogeneous radio frequency (RF) fields are important for sensitivity and efficiency of magnetization transfer in solid state NMR experiments. If the fields are inhomogeneous the cross polarization (CP) experiment transfers magnetization in only a thin slice of sample rather than throughout the entire volume. Asymmetric patterns have been observed in plots of the CP signal versus RF field mismatch for an 800 MHz solid-state NMR probe where each channel is resonated in a single-ended mode. A simple model of CP shows these patterns can be reproduced if the RF fields for the two nuclei are centered at different places in the coil. Experimental measurements using $B_1$ field imaging, nutation arrays on extremely short NMR samples, and de-tuning experiments involving disks of copper incrementally moved through the coil support this model of spatially offset RF fields. We have found that resonating the high frequency channel in a double-ended or ''balanced'' mode can alleviate this field offset problem, and have implemented this in a three-channel solid state NMR probe of our own design.


*Keywords:* Cross polarization; Magic angle spinning; NMR probe; RF field; RF homogeneity

## 1. Introduction

Many techniques in NMR spectroscopy, especially in solid-state NMR, rely on applying radio frequency (RF) fields ($B_1$) on two or more channels to nutate the different nuclei at well-defined rates relative to each other. One important example is cross polarization (CP), which is commonly used to transfer magnetization between different nuclei. In CP one applies $B_1$ spin-locking fields simultaneously to two different nuclei such that the respective Rabi frequencies are equal, $\omega_{1I} = \omega_{1S}$, the so-called Hartmann–Hahn matching condition. This condition makes mutual spin flips via the dipolar coupling between two spins energy conserving, permitting the magnetization of the two nuclei to equilibrate. CP is commonly used to transfer magnetization from a nucleus $I$ such as $^1$H with a high gyromagnetic ratio, $\gamma_I$, to a nucleus of interest $S$, gyromagnetic ratio $\gamma_S$, often $^{13}$C or $^{15}$N. Efficient magnetization transfer can only take place when the $B_1$ field mismatch parameter, $\Delta = \omega_{1I} - \omega_{1S}$, is set close to zero. The degree of precision with which $\Delta$ must be set depends on the size of the effective heteronuclear dipolar coupling. As long as $\Delta$ is small compared to the dipolar couplings, cross polarization can take place.

When CP is combined with magic angle spinning (MAS) the dipolar interaction becomes time dependent. For a given MAS rate $\omega_r$, the most efficient transfer then occurs not when $\Delta$ is close to zero, but rather when $\Delta$ is close to either $\pm\omega_r$ or $\pm 2\omega_r$. This is typically referred to as a sideband matching condition [1,2]. To maintain spinlocked magnetization it is also important to avoid matching the RF field nutation rates $\gamma_i B_1$ to $\omega_r$ or $2\omega_r$, otherwise the spinlocked magnetization can be destroyed by recoupling of the chemical shift anisotropy

* Corresponding author. Fax: +1 203 432 6144.
*E-mail address:* kurt.zilm@yale.edu (K.W. Zilm).

1090-7807/$ - see front matter © 2004 Elsevier Inc. All rights reserved.
doi:10.1016/j.jmr.2004.09.009

[3]. In practice these considerations and the requirements for efficient $^1$H decoupling make application of RF fields where $\gamma_i B_1 > 5\omega_r$ advantageous [4]. At high spin rates $\Delta$ becomes a significant fraction of $\gamma_i B_1$, placing very stringent demands on the homogeneity of the applied RF fields.

As the $^1$H operating frequency of the NMR spectrometer increases to 800 MHz and beyond, the MAS rates employed approach or even exceed typical $^1$H–$^{13}$C and $^1$H–$^{15}$N one bond dipolar couplings. In this instance RF field inhomogeneity effects on magnetization transfer via CP become even more important, and are a serious impediment to maximizing sensitivity. Some of the methods that have been used to ensure homogeneous $B_1$ fields include restricting the sample to the central region of the detection coil [5], winding the sample coil with a variable pitch or width of wire [6–8] and utilizing a single sample coil that is resonant at all the frequencies of interest. Probes used in our laboratory at $^1$H NMR frequencies of 300 MHz have employed these features and provide for reasonably efficient CP transfers, even at high MAS rates (>20 kHz) on samples with small effective heteronuclear dipolar couplings such as adamantane. However, in constructing a triple-resonance probe operating at a $^1$H frequency of 800 MHz, CP transfer was found to be quite inefficient in comparison to that routinely achieved at lower operating frequencies. In addition to the lesser signal enhancement obtained with CP, the matching condition was found experimentally to be poorly defined, with some degree of CP possible for a very wide range of $\Delta$ values.

These symptoms have been found to be the result of RF field inhomogeneity caused largely by what we will call finite wavelength effects. The latter are a consequence of the fact that the wire in the probe coil, although very short, is in fact not that short when compared to the wavelength corresponding to the $^1$H resonant frequency [9]. To characterize these effects we have measured the $B_1$ field profiles of each channel in our probe using $B_1$ field imaging, nutation arrays on extremely short NMR samples incrementally positioned through the coil, and de-tuning experiments involving slugs of ferrite or copper incrementally moved along the axis of the coil. A marked difference in the $B_1$ field profile of the high frequency channel relative to the lower frequency channels is observed even though the same coil is producing these $B_1$ fields in a typical circuit configuration. Operating the high frequency channel in a balanced mode is found to largely eliminate these effects.

The salient features of this problem are most readily understood if we first consider the effects of RF field inhomogeneity on the CP dynamics of an isolated spin pair, and some basic circuit equations for resonant RLC circuits. We begin with a brief review of each aspect.

## 2. Cross polarization of an IS spin pair under fast MAS

Close to one of the $k = \pm 1$ or $\pm 2$ sideband matching conditions, the spinlocked $S$-spin magnetization $S_x(\tau)$ created for an isolated IS spin pair by cross polarization in a time $\tau$ under fast MAS is well described [2] by

$$\langle S_x(\tau)\rangle = \frac{|b_k|^2}{|b_k|^2 + (\Delta - k\omega_r)^2}\sin^2\left\{\frac{\tau}{2}\sqrt{|b_k|^2 + (\Delta - k\omega_r)^2}\right\}. \tag{1}$$

In Eq. (1), the $b_k$ are the Fourier components of the time dependent heteronuclear dipolar coupling $b(t)$:

$$b(t) = \sum_{k=-2}^{2} b_k e^{i\omega_r t}, \tag{2}$$

where

$$b_{\pm 1} = -b_{IS}\sqrt{2}\sin(2\beta)e^{\pm i\gamma}, \tag{3}$$

$$b_{\pm 2} = -b_{IS}\sin^2\beta e^{\pm 2i\gamma}, \tag{4}$$

and

$$b_{IS} = \frac{\mu_o}{4\pi}\frac{\gamma_I\gamma_S\hbar}{4r^3}(\text{rad s}^{-1}). \tag{5}$$

The angle $\beta$ is between the IS internuclear vector and the rotor axis, and $\gamma$ gives the starting orientation of this vector as it rotates around the rotor axis. This expression is a good description of the CP dynamics under fast MAS with large RF fields, taken here to be when $|b_k| < \omega_r$ and when $(\omega_{1I} + \omega_{1S}) \gg \omega_r$. For a fixed CP time $\tau$ the magnetization created is maximized at the sideband matching conditions where $\Delta = k\omega_r$, $k = \pm 1$ or $\pm 2$.

Experimentally finding the best CP match involves obtaining a matching curve, a plot of signal strength obtained at a fixed $\tau$ while one of the RF field amplitudes is varied and the other is held constant. When the MAS rate and the RF fields are large and the dipolar coupling is small, the amount of magnetization that can be transferred is dominated by the prefactor in Eq. (1). In this case, the envelope of the matching curve will depend strongly on the details of how the RF field varies across the sample. For a sample such as adamantane with a small effective dipolar coupling, we can replace the $b_k$ by their powder weighted averages over $\beta$, $\bar{b}_k$, and sum the contributions from $k = \pm 1$, $\pm 2$ if the MAS rate is fast. The envelope function, which we will denote as $S(\Delta, \omega_r, b_{IS})$, is then approximately

$$S(\Delta, \omega_r, b_{IS}) = \sum_k \frac{|\bar{b}_k|^2}{|\bar{b}_k|^2 + (\Delta - k\omega_r)^2}. \tag{6}$$

Computer simulations of this envelope function integrated over the sample volume are shown in Fig. 1 for a variety of parameters. In each instance the RF field amplitude has been modeled as a Gaussian profile over

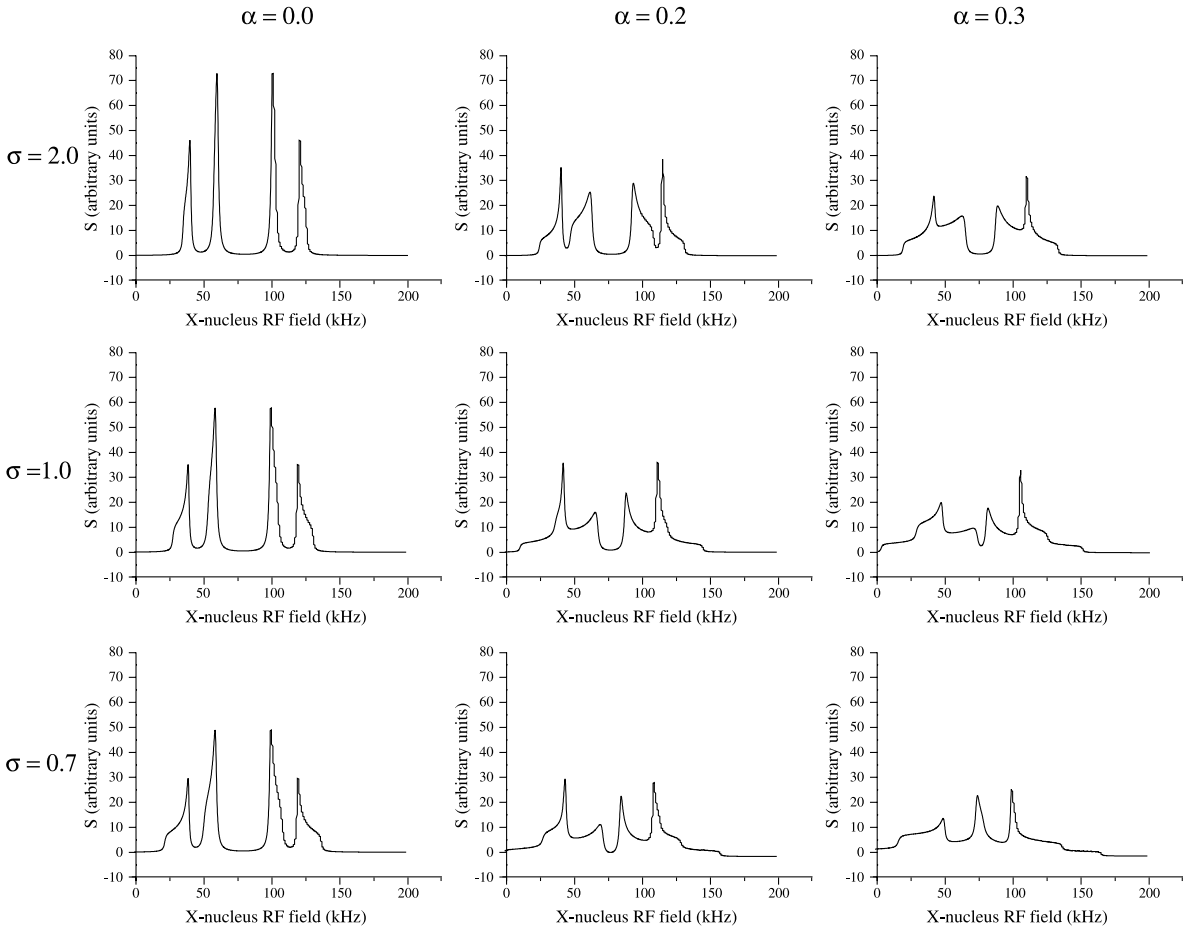


Fig. 1. Matrix of matching curve integrated envelope functions $S$ calculated as described in the text for different fractional offsets α of the $^1$H RF field center relative to the sample center, and for different levels of RF homogeneity as parameterized by $\sigma$. A more familiar measure of the RF homogeneity is the size of the signal obtained with an 810° pulse in comparison to a 90° pulse. The $\sigma$ values 2.0, 1.0, and 0.7 correspond to 810°/90° ratios of 90, 65, and 40% respectively. For each curve the $^1$H field was left fixed, and the amplitude of the X-nucleus RF field incremented ($X$-axis). The $\sigma$ values for both fields were assumed to be the same. In these simulations $b_{IS}/2\pi = 4000$ Hz, the spin rate was set to 20 kHz, and the maximum amplitude in the $^1$H RF field profile set at 80 kHz. The upper left hand profile shows the expected set of 4 sideband matching conditions when the X nucleus RF field is set to 40, 60, 100, and 120 kHz, corresponding to the $\Delta = \omega_{1X} - \omega_{1H} = -2\omega_r$, $-\omega_r$, $\omega_r$, $2\omega_r$ conditions, respectively.

the sample spanning a dimensionless length $\ell$ from +0.5 to −0.5, and having the functional form $B_1(\ell) = B_{1\,\max}e^{-(\ell+\alpha)^2/\sigma}$. A set of such RF field profiles are plotted in Fig. 2 for the case where the X(S) and $^1$H($I$) fields have coincident centers ($\alpha = 0$), and where there is a finite offset in the profiles. The parameter $\sigma$ defining the width of the Gaussian RF profile is a convenient way to specify the RF inhomogeneity in simulations as described in the captions to Figs. 1 and 2. The X-nucleus field in Fig. 2 has been set to a maximum amplitude $\gamma B_{1\max}/2\pi$ of 80 kHz. When using MAS at 20 kHz, the $^1$H field needs to be set at some multiple of 20 kHz above or below this. Since the RF field profile is not flat across the sample, such a condition cannot be met simultaneously everywhere at once. Therefore, when the average dipolar coupling is not large enough, different parts of the sample will match for different values of $B_{1\max}$. In the centered case the $^1$H field is shown that best provides for a $\Delta/2\pi$ of −20 kHz across the largest portion of the sample. For the shifted $^1$H field case ($\alpha = 0.2$) the best match occurs in a very different condition. In this situation the field most easily produces the proper $\Delta$ for the right hand end of the sample.

The integrated matching envelopes in Fig. 1 for several combinations of α and $\sigma$ show how important it is to have coincident field centers for efficient CP transfer. As the RF field across the sample becomes less homogeneous, each of the CP matching resonances broadens out into the shape of an axially symmetric powder pattern, with the center of the sample being the peak of intensity and the outer wings corresponding to the ends.

Moving from left to right in Fig. 1 the misalignment of the RF fields is increased. When the RF field centers are no longer coincident the matching curve loses its reflection symmetry about the $\Delta = 0$ condition, and the match conditions broaden excessively. At the same time the peak intensity that is available drops as it is not possible to get all portions of the sample to partici-

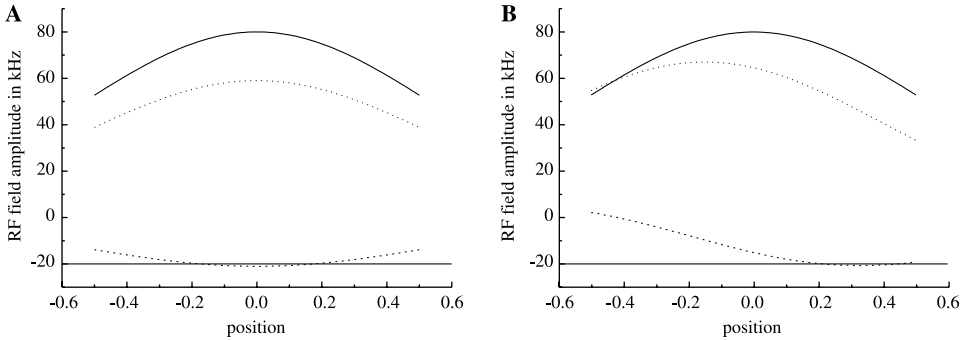


Fig. 2. Spatial profiles of RF fields close to a sideband matching condition illustrating the effect of a non-centered $^1$H RF field. (A) The fields are centered while in (B) the $^1$H field center is shifted by 0.15 of the sample length. The RF fields are calculated as Gaussians of the form $\frac{\gamma B_1}{2\pi} = \frac{\gamma B_{1\max}}{2\pi} e^{-(\ell+\alpha)^2/\sigma}$, where $\ell$ is the position in the coil, $\alpha$ the offset from the coil center of the RF field, and $\sigma$ determines how strongly the RF field profile varies across the sample. In both cases the X-nucleus field (solid line) is computed as centered ($\alpha_X = 0$), has a maximum amplitude of 80 kHz, and $\sigma = 0.6$. This $\sigma$ value was chosen to be illustrative, useful probes have $\sigma$ values of 2 or greater. For a centered field, a $\sigma$ of 2.0 produces a RF field which will give a 810°/90° ratio of 90%. A $\sigma$ of 0.6 produces a RF field where the 810°/90° ratio is computed to be less than 40% (not accounting for signal detection). The $^1$H fields (dotted line) have maximum amplitudes chosen to best satisfy a matching condition $\Delta = \omega_X - \omega_H = \omega_r$ over the largest sample volume when the MAS rate is 20 kHz. For the centered case in (A) the maximum $^1$H RF amplitude is 59 kHz, while in the offset example in (B) the maximum $^1$H field is 67 kHz. The $\Delta$ values are also shown as dashed lines, with a thin solid line at −20 kHz drawn to aid the eye in recognizing the region where a CP match is best satisfied.

pate in CP at the same time. These envelope curves mimic quite well the behavior observed in this type of experiment when adamantane is used as the test sample (vide infra).

The increased signal obtained using variable amplitude or ramped CP transfers [10] is often a result of dealing with this sort of RF inhomogeneity problem. In a ramped CP experiment the ramp can be set to sweep across one of these broad matching resonances, and as long as $T_{1\rho}$ is long enough the spinlocked magnetization transfer greatly increased. If a field center misalignment is present the problem is more severe. In this instance restricting the sample size can do little to improve the RF field profile. The only solution then is to insure that the fields do in fact have as close to the same spatial profile as possible.

## 3. Basic AC circuit theory and balancing in multiply resonant RLC circuits

The fact that the RF field from a simple finite length solenoid is inhomogeneous is well known. It is less well known however that the RF field profile does not have to be symmetric about the coil center, even at moderate frequencies. Once the length of wire in the coil becomes ~10% of the wavelength, there can be significant departures from the direct current field profile. The first experimental observation of this phenomenon we are aware of was a report by Stuhlman and Githens [11]. More recently this issue has been investigated using modern computational approaches by Engelke [9].

In our 800 MHz triple resonance probe the coil consists of 6 turns with an inner diameter of 0.12 in., and including the lead lengths is made of a wire about 9 cm in length, or nearly 25% of the free space wavelength $\lambda$ at 800 MHz. At the $^{15}$N and $^{13}$C frequencies the wire is 2.4 and 6% of the wavelength, respectively. While we might justifiably anticipate idealized behavior when this coil is driven at either of these frequencies, we should not expect this to be the case at the $^1$H frequency. When wavelength effects become important, a finite length wire wound inductor will produce a $B_1$ field which does not reflect the symmetry of the coil. Reflection symmetry of the field can however be restored if the inductor is resonated in a balanced mode, as is well known in the NMR imaging field [12].

The difference between an unbalanced probe and a balanced probe can be readily understood using basic AC circuit theory. For simplicity first consider the case where the RF frequency is not so high that wavelength effects are an issue. In this instance the instantaneous current $\vec{i}(t)$ can be taken as the same at all points in a simple RLC circuit. The steady state current–voltage relation across any single component is then fixed by the complex impedance through $\vec{v}_{kl}(t) = Z_{kl}\,\vec{i}(t)$. For a resistor $Z = R$, for an inductor $Z = j\omega L$, and for a capacitor $Z = -j/\omega C$, where we have used $j = \sqrt{-1}$ to avoid confusion with $\vec{i}(t)$. Now consider the example circuit in Fig. 3A. The voltage source provides a voltage $v(t) = v_{ad}(t) = v_0 e^{j\omega t}$, and the net series impedance is $Z_{ad} = Z_c + Z_L + Z_R = j\omega L + 1/j\omega C + R$. If the frequency $\omega$ is chosen as the resonant frequency, $LC = 1/\omega^2$, $Z_{ad} = R$, and $\vec{i}_{ad}(t) = \vec{i}_{cd}(t) = \vec{i}(t) = v(t)/R$.

The voltage across the capacitor $C$ is then $v_{ab}(t) = -(j/\omega C)\,\vec{i}(t)$. Substituting for the current gives $v_{ab}(t) = (1/\omega CR)\,v(t)\,e^{-j\pi/2}$. If the resistance $R$ is taken to be the equivalent series resistance for the inductor $L$, we can substitute using the definition of the quality factor $Q = \omega L/R$. At resonance $\omega L = 1/\omega C$, therefore the

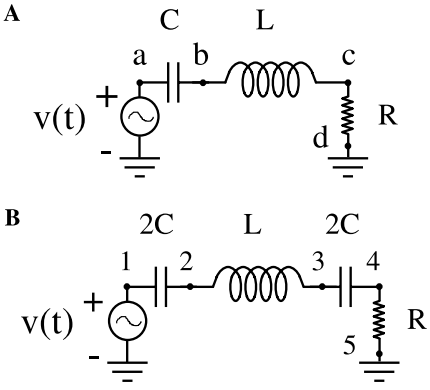


Fig. 3. (A) Unbalanced series resonant circuit and (B) balanced series resonant circuits discussed in text.

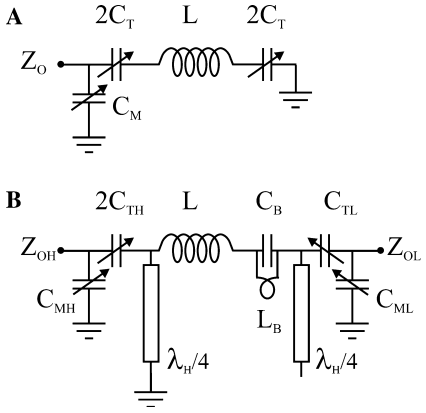


Fig. 4. (A) A balanced tuned and matched single resonance probe circuit. (B) Double resonance probe circuit balanced in the high frequency channel by use of a balancing trap.

voltage across the capacitor at resonance is $v_{ab}(t) = Qv(t)\ e^{-j\pi/2}$, or $Q$ times the applied voltage and out of phase by $-\pi/2$. It likewise follows that the voltage across the inductor $v_{bc}(t) = j\omega Lv(t)/R$ or $Qv(t)\ e^{+j\pi/2}$. Thus $v_{bc}(t) = -v_{ab}(t)$, and $v_{ac}(t) = 0$ as expected for a simple series resonant circuit.

In the circuit shown in Fig. 3B the same inductance and resistance are used, but the capacitance is now split across the inductor. This circuit has the same resonance frequency as $Z_{14} = -j/2\omega C + j\omega L - j/2\omega C = -j/\omega C + j\omega L = Z_{ac}$. Therefore the current is the same for the same $v(t)$ and $v_{12}(t) = (Q/2)\ v(t)\ e^{-j\pi/2}$. The voltage across the inductor is still the same, $v_{23} = Q\ v(t)\ e^{+j\pi/2}$, and the voltage across the second capacitor is $v_{34} = (Q/2)v(t)\ e^{-j\pi/2}$. As before, since the circuit is resonant, the voltage across the entire circuit $v_{14} = 0$.

The main difference between the two circuits arises when the voltages at the various points are considered relative to the ground plane. In the first circuit the voltage $v_{bd}$ at the junction of the capacitor and inductor relative to ground is $v_{bc} + v_{cd}$. As long as R is small, i.e., $Q$ high, $v_{bd} \sim v_{bc} = Q\ v(t)\ e^{+j\pi/2}$. In the second circuit the voltage relative to ground at the first junction is $v_{23} + v_{34} = (Q/2)\ v(t)\ e^{+j\pi/2}$, while at the second junction this is $v_{34} = (Q/2)\ v(t)\ e^{-j\pi/2}$. The voltage rise with respect to ground then is half the amplitude of that in the single ended circuit. Both ends of the inductor experience the same voltage swing with respect to the ground plane, but these are out of phase by $\pi$ at any point in time.

The advantage of the double-ended or "balanced" circuit is that the inductor is symmetrically driven. This will largely be true even if the inductor is not an ideal element. The importance of using a balanced configuration is that in this case the symmetry of the $B_1$ field is restored by making the voltage swings at the ends of the inductor symmetrical when measured relative to ground.

The circuit for a balanced single frequency impedance matched probe circuit is depicted in Fig. 4A. The tuning capacitance $C_T$ required to resonate the coil inductance $L$ is simply split across the inductor, and the circuit is matched with a capacitance $C_M$. To extend this approach to probe circuits where a single coil is resonated at multiple frequencies, additional elements are needed. Fig. 4B outlines one possible approach to a double resonance probe circuit that is balanced on the high frequency (hf) side. In this circuit a pair of $\lambda_H/4$ resonant transmission lines are used to provide different ground paths for the high and low frequency (lf) currents. The shorted $\lambda_H/4$ line represents a high impedance to the hf input, while it appears as a small series inductance for the lf channel. The open circuit $\lambda_H/4$ line appears as a series resonant trap or a ground path to the hf current. This same transmission line appears capacitive to the lf channel.

In hf mode the inductor $L$ is tuned and matched as in the previous circuit, with the ground path being through the shorted $\lambda/4$ line. The second half of the tuning capacitance $C_{TH}$ is provided by the balancing trap consisting of $C_B$ and $L_B$. These two components are chosen such that their parallel combination presents a reactance equivalent to that of the tuning capacitor $2C_{TH}$ at the hf. Low frequency operation tunes and matches the sample coil inductance $L$ with $C_{TL}$ and $C_{ML}$. In this mode the open $\lambda_H/4$ line adds a small capacitance in parallel with $C_{TL}$, and the shorted line provides a low impedance inductive ground path. The balancing trap appears as a small additional inductance in series with $L$ in lf mode.

Incorporation of a parallel balancing trap to balance the hf side of a multiple resonance probe is a rather general approach not limited to the particular circuit used here for discussion. The choice of $L_B$ and $C_B$ can be guided by considering the impedance $Z_B$ of their parallel combination

$$\frac{1}{Z_B} = j\omega C_B + \frac{1}{r + j\omega L_B}, \tag{7}$$

where $r$ is taken as the equivalent series resistance of $L_B$. Tuning the trap to a resonance frequency $\omega_B = 1/\sqrt{L_B C_B}$ in between the lf and hf channel frequencies results in a reactance in the hf band that is purely capaci-

tive, while appearing inductive to the low frequency channels. For any realistic component values $r$ can be set to zero as long as we only consider frequencies at least a few percent away from $\omega_B$. The effective net inductance and capacitance are then

$$L_{\text{eff}} = \frac{L_B}{1-\omega^2 L_B C_B} \quad \text{for } \omega < \omega_B,$$
$$C_{\text{eff}} = C_B - \frac{1}{\omega^2 L_B} \quad \text{for } \omega > \omega_B. \tag{8}$$

To minimize the impact on probe efficiency, $L_B$ should be chosen small, and made as high $Q$ as possible. $C_B$ can conveniently be made fixed, and the trap resonance frequency tuned by stretching or compressing the inductor windings.

In our $^1H/^{13}C/^{15}N$ triple resonance probe the sample coil has an inductance of approximately 70 nH. The balancing trap consists of an inductor made from 3 turns of 16 gauge wire wound on a 0.125 in. diameter form, having an inductance of ~14 nH. This is resonated in the vicinity of 700 MHz by a fixed capacitor made from a length of Teflon dielectric coaxial cable [13] with an inner conductor diameter of 0.125 in. Fig. 5 depicts how the effective inductance and capacitance of this structure varies with frequency, as simulated using the Hewlett–Packard electronics design package Touchstone for Windows, version 2.2, as we have also described elsewhere [13]. Although the coaxial capacitor has a capacitance of ~4 pF in the vicinity of 800 MHz, the combination of this capacitor with the balancing inductor provides a reactance equivalent to the 1.12 pF capacitor required for balanced operation of the circuit.

Fig. 6 displays circuit simulation results for the voltage swings across the sample inductor in the full triple resonance probe circuit for the hf band, tuned with and without the balancing trap as just described (see Fig. 6 in [13] for the complete circuit diagram). Voltages corresponding to the test points labeled on the single-ended circuit in Fig. 3A are displayed in the plot in Fig. 6A. The small voltage to ground for the coil lead ($|V_{cd}|$) arises due to the finite impedance to ground taken into account in the simulation. The plot in Fig. 6B is the simulation for the same circuit with the addition of the balancing trap, and retuned to resonate at the same three frequencies. Test points are labeled here as in Fig. 3B. The voltage at one end of the coil is 180° out of phase with the other end as expected, while the total voltage across the coil is as high as obtained in single ended mode. Use of an accurate computer simulation model proved indispensable in implementing balanced hf channel operation in this complex circuit.

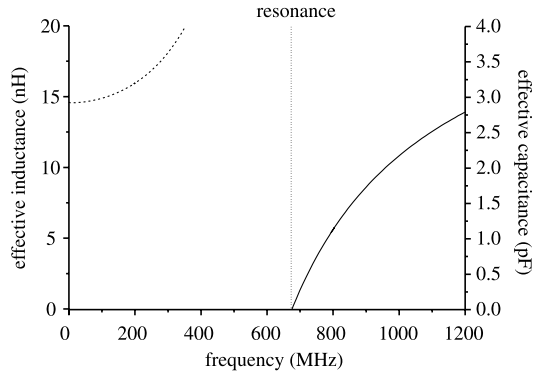


Fig. 5. Reactance of the balancing element described in the text as a function of frequency. This trap resonates close to 700 MHz as indicated. Below this frequency the reactance is inductive, and the equivalent inductance is given by the dashed curve and axis on the left. Above 700 MHz the reactance is capacitive, with the effective capacitance plotted by the solid line with the value indicated by the axis to the right.

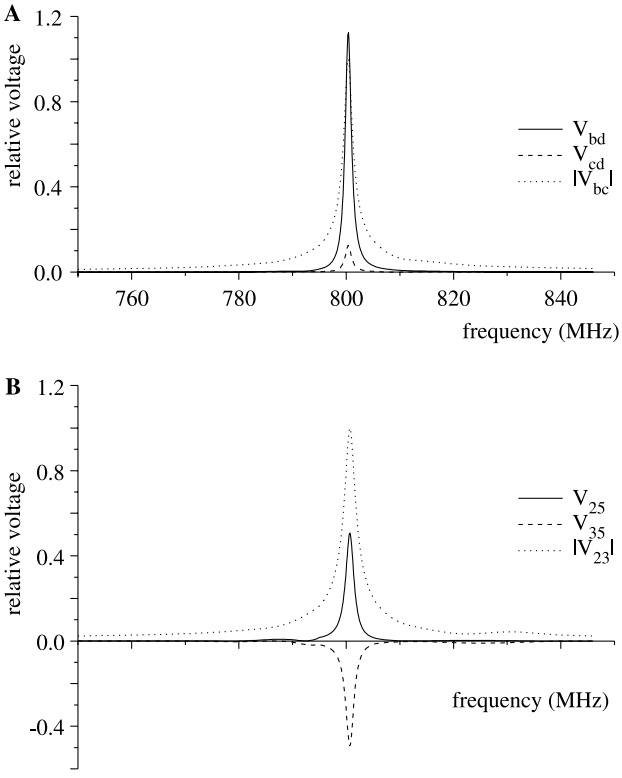


Fig. 6. Computed voltage rise across sample coil or between indicated points and ground as a function of frequency. (A) For coil in the full triple resonance circuit diagrammed in Fig. 6 of [13], tuned and matched, but without the balancing trap. Test points in the circuit correspond to labels used in Fig. 3A. In this case all the voltages have the same phase relative to the applied RF. (B) depicts what is calculated when the circuit is tuned and matched with the balancing trap in place and properly adjusted. The voltages $V_{25}$ and $V_{35}$ to ground are the same magnitude but are 180° out of phase with each other, as represented by plotting $V_{35}$ as negative. The magnitude of the total voltage swing across the inductor $|V_{23}|$ is then twice as large as that at either end with respect to ground in the balanced configuration.

## 4. Experimental verification

The first indication that the hf RF field was not centered at the same position in the sample coil as the X nucleus RF field is in our 800 MHz triple resonance probe

came from characterizing the RF homogeneity in the $^{1}H$ and $^{13}C$ channels. Initially we thought that poor $B_1$ homogeneity resulted from not having the sample centered. The center-to-center distance between the outermost turns of the coil is $\sim 0.210$ in., and the sample is only 0.150 in. in length. Therefore a miscalculation of only 0.050 in. in positioning the sample represents a shift relative to the coil center by 1/3 of the overall sample length. Changing the sample position indeed did improve the RF homogeneity in one channel, but only at the expense of the other. This eventually led us to the conclusion that the $^{1}H$ RF field was not centered on the sample coil. To independently verify this initially surprising conclusion a number of independent measurements were undertaken.

## 5. Nutations on thin samples and resonance shift measurements

A 1 mm thin slice of adamantane was incrementally moved through the MAS rotor to map out the $^{1}H$ and $^{13}C$ RF field amplitudes along the rotor axis. A series of Kel-f sample spacers were machined to make it possible to accurately move the tightly packed disk of adamantane from one end of the coil to the other. At each position the $^{1}H$ and $^{13}C$ RF field amplitudes were determined by measuring a nutation curve over three cycles. The results are plotted in Fig. 7A. This simple but tedious measurement unambiguously demonstrated the two RF fields had very dissimilar spatial profiles.

Electronic measurements of the $B_1$ field were also performed by incrementally moving a small disk of copper through the inside of a zirconia rotor in place in the NMR probe. The shift of the tuning frequency $\Delta\omega/2\pi$ caused by the conductive perturbation is proportional to the square of the $B_1$ field at that point [14]. Positioning the disk in the coil was accomplished in a reproducible fashion using the Delrin fixture diagrammed in Fig. 8. This fixture consists of a threaded plate through which a 4-40 nylon machine screw can be advanced. The perturbing disk is connected to the screw by a length of Teflon heat-shrink tubing that extends beyond the coil. In this manner the disk can be moved without also changing the dielectric constant of the supporting structure inside the coil. The disk was positioned in steps of one complete revolution of the nylon screw in an attempt to avoid any effects due to the orientation of the disk. At each increment the resonant frequency of the probe was monitored using a RF sweep generator, reflection bridge and a spectrum analyzer. Results without the balancing element are shown in Fig. 7B. While the $^{13}C$ channel at 200 MHz displays a very symmetrical profile, the 800 MHz $^{1}H$ channel has a distinct asymmetry.

Adding the balancing trap dramatically changes these measured field profiles. In Fig. 7C the electronic measurements are repeated, demonstrating that the RF

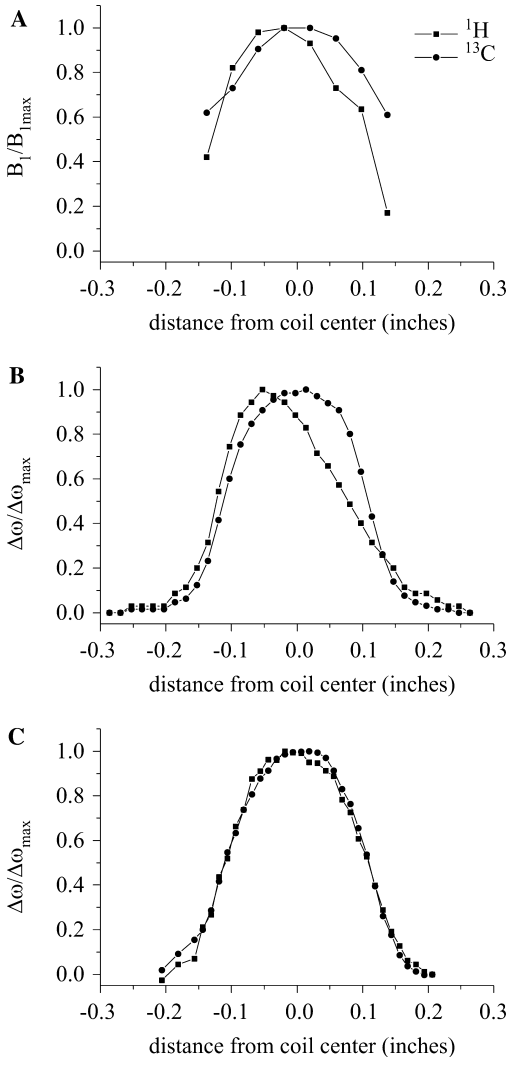


Fig. 7. Measurements of axial $^{1}H$ and $^{13}C$ $B_1$ fields as function of position within the sample coil. (A) In probe without balancing as measured by nutations on a thin slice of adamantane. (B) In same probe without balancing but assessed by measuring probe resonance shift as a function of the position of a very small perturbing copper disk. (C) Measured as in (B) but now with the probe balanced in the high frequency channel.

fields for the $^{1}H$ and $^{13}C$ fields are in much better alignment. Since the electronic test provides the same information as the nutation experiment, this has become the primary diagnostic used in our laboratory when initially balancing a probe circuit.

## 6. Imaging of RF field profiles by nutation and CP matching conditions

Direct images of the $B_1$ fields for the $^{1}H$ and $^{13}C$ channels were generated for a sample of $^{13}C$ labeled glycine under magic angle spinning (MAS) in the presence of a static magnetic field gradient along the main applied field. The gradient was produced by simply moving the

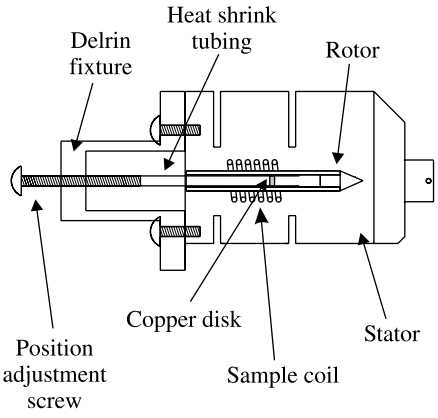


Fig. 8. Apparatus for electronically measuring the magnetic field profile inside the rotor, shown in cross section as affixed to the Chemagnetics 2.5 mm MAS stator. As the copper disk is incrementally positioned along the axis of the rotor by advancing the screw, the tuning frequency is monitored on the channel of interest. Frequency deflections are proportional to the square of the magnetic field at each point in the coil.

probe to a position approximately 4 cm below the center of the $B_0$ field. The spectrum was acquired as a function of the nutation time $t_1$, and an image obtained using a Fourier sine transform. The same position was used for all measurements where the gradient broadens each of the two lines the $^{13}$C glycine spectrum into rectangular profiles of approximately 20 kHz, or 100 ppm in width. The $B_1$ field images (not shown) confirm the $^1$H field profile is asymmetric and the $^{13}$C field profile symmetric without the balancing element, and that both become symmetrical and aligned with balancing.

A much more sensitive measure of the alignment of the two RF fields can be produced using the CP matching condition to ascertain $\Delta$ as a function of position in the sample. In this experiment a static magnetic field gradient was produced with a component along the axis of the MAS rotor by adjusting the room temperature shims in the proper combination [15]. This gradient was set to broaden the two lines in the $^{13}$C MAS spectrum of adamantane to rectangular profiles of ~500 Hz, or 2.5 ppm. Since the gradient is along the rotor axis, there is a one to one correspondence between resonance frequency of any particular isochromat and the spatial location of the corresponding portion of the sample. High power $^1$H decoupling was applied and the MAS rate was set to ~19 kHz. A CP matching array was then acquired in the presence of this gradient by sequentially stepping the RF power in one channel through a sideband matching condition while leaving the RF power in the other channel fixed. When arranged in a stacked plot this gives a profile that indicates how $\Delta$ varies as a function of location in the sample along the rotor axis.

The results of the $\Delta$ versus location imaging experiment are shown in Fig. 9 for both an unbalanced (A) and a balanced (B) high frequency channel. Reference to the field profiles in Fig. 2 readily explains the patterns seen. In the balanced case shown in Fig. 9B, the fields are centered on the coil together. When the $^{13}$C RF field amplitude in the center of the sample $\Delta_0$ is adjusted to satisfy $(\omega_{1H} - \omega_{1C})/2\pi = 19$ kHz, $\Delta$ will be less than this at the sample ends. To cross polarize the outermost portions of the sample, the $^{13}$C power must be lowered to satisfy the same $k = +1$ sideband matching condition

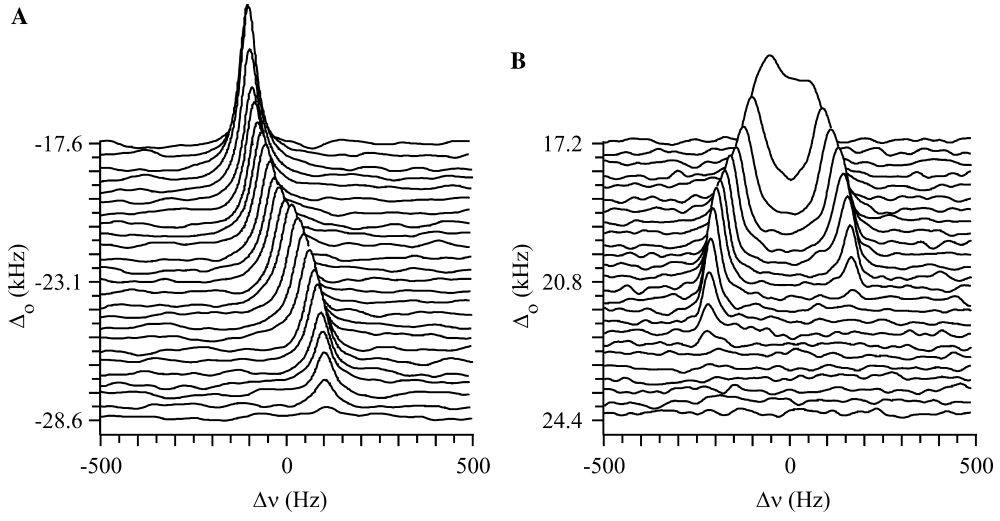


Fig. 9. Comparison of CP matching images for an unbalanced probe and a probe with a balanced high frequency channel. Both plots show the matching condition for a single $^{13}$C resonance in adamantane with the MAS rate set at 19 kHz in a static field gradient. (A) Unbalanced matching array in a static field gradient. The value of $\omega_{1C}/2\pi$ at the coil center was fixed at 70.2 kHz, and $\omega_{1H}/2\pi$ at this position stepped from 41.6 to 52.6 kHz.This sweeps through the $\Delta/2\pi = (\omega_{1H} - \omega_{1C})/2\pi = -19$ kHz sideband match. (B) Balanced matching array in a static field gradient. $\omega_{1H}/2\pi$ at the coil center was fixed at 52.6 kHz and $\omega_{1C}/2\pi$ at this position stepped from 28.3 to 35.4 kHz. This sweeps through the $\Delta/2\pi = (\omega_{1H} - \omega_{1C})/2\pi = +19$ kHz sideband match. The larger area at the optimal matching condition in the balanced case corresponds to higher signal to noise in standard operation. The CP time used in these experiments was 3 ms. The vertical axis in both plots is labeled by $\Delta_0$, the value of $\Delta$ at the coil center.

there. At this lower $^{13}C$ power level the $\Delta_0$ value in the center of the sample is then $>\omega_r$, and the signal from the center of the sample disappears. In the matching array the signals corresponding to the ends of the sample then match at the lowest $^{13}C$ power level (largest $\Delta_0$). As the matching power is raised sample portions successively closer to the middle match, until finally the center of the sample matches and the signal disappears as the power is increased further.

Using an unbalanced configuration results in the RF fields being miscentered and changes the results dramatically. Data in this case for the $\Delta$ versus location imaging experiment around the $-1$ sideband match are shown in Fig. 9A. In this instance the $^{13}C$ power was held fixed while the $^{1}H$ power level was incremented through the $k=-1$ sideband match. The condition producing the largest signal corresponds to a situation that must be similar to that plotted in Fig. 2B. At this setting the $\omega_{1H}-\omega_{1C}=-19$ kHz condition (smallest absolute value of $\Delta_0$) is matched at one end for a considerable fraction of the sample due to the approximately parallel field profiles. As the $^{1}H$ power is decreased further this portion goes out of match, while new portions of the sample come into the matching condition. The progression moves linearly through the sample, with the fraction of the sample that can be matched ever decreasing. The matching array in this case then starts with a large signal (upper traces in array) that quickly shrinks as $\omega_{1H}$ is decreased (traces towards the bottom of Fig. 9B). The larger signal area at the optimal matching condition in the balanced case corresponds to higher signal to noise in standard operation.

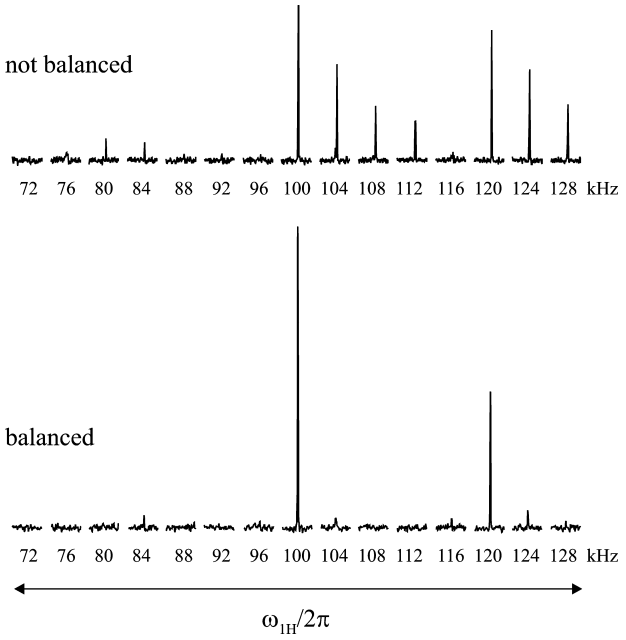


Fig. 10. Comparison of CP matching arrays. $^{13}C$ MAS spectra of the methylene resonance in adamantane at 20 kHz MAS as a function of the $^{1}H$ CP RF field amplitude. Upper: for a probe not balanced in the hf channel. Lower: for the same probe with a balanced hf channel. The larger volume of sample that can be cross polarized in the balanced probe at a single power setting translates into a much higher ultimate signal-to-noise. A 1 ms CP time was used to acquire these data and $\omega_{1C}$ fixed at 80 kHz.

## 7. CP matching arrays

As a final result we return to a comparison of the matching curve obtained with a balanced probe versus one that is not. Fig. 10 shows the $^{13}C$ signal for the methylene carbon in adamantane as a function of the apparent $^{1}H$ $B_1$ field with $\omega_r/2\pi$ set to 20 kHz. The size of $\Delta$ was adjusted by keeping $\omega_{1C}/2\pi$ fixed at 80 kHz at the coil center, while arraying the proton power level to vary $\omega_{1H}/2\pi$ at this position from 72 to 128 kHz in steps of 4 kHz. The matching conditions for the balanced probe are significantly narrower and more intense than obtained in the unbalanced probe, giving a signal to noise improvement of approximately 2 for the optimal matching condition in each configuration. The envelopes of these matching curves follow the trends expected from the simulations in Fig. 1.

## 8. Conclusions

Wavelength effects can produce a significant misalignment of the physical centers of the RF fields produced in a single coil probe tuned to multiple frequencies. For a solenoidal coil this becomes experimentally important once the length of wire is 10% or more of the hf wavelength. This causes RF field homogeneity related problems in CP experiments, especially at high spin rates. Balancing the hf channel ameliorates these problems to a large extent. The balanced circuit configuration does result in lesser efficiency due to the extra circuit elements required in the probe. This loss proved to be greatest for the $^{1}H$ channel here, where as a result the $\pi/2$ pulse time increased by $\sim$15% for the same applied power. However, this decrease in efficiency is much more than compensated for by the improved RF homogeneity and enhanced CP performance.

The difficulties with RF field profiles in CPMAS probes reported here should not be only expected at high fields. A large sample CPMAS probe for a 7.0 T instrument might have an 8-turn coil wound on a 8 mm diameter form of 10 mm in length. The coil wire length in this case would be $\sim$220 mm, or 22% of the $^{1}H$ wavelength, and would therefore be expected to pose the same difficulties as we have encountered on our 800 MHz system. One of the advantages often attributed to a single coil multiple resonance probe is that the RF field profiles for the different nuclei will be the same. As we have demonstrated here this is not necessarily true without balancing of the high frequency channel. At

one time crossed coil probes were thought to be at a disadvantage for CPMAS NMR in this regard, but this should no longer be considered a serious detraction in comparison [16]. Imaging of the CP matching condition at a high MAS rate on a sample with small dipolar couplings provides a sensitive measure of the spatial mismatch in RF fields, and this type of measurement can be used to evaluate the relative merit of any double resonance probe design in this regard.

In conclusion, the combination of high MAS rates and wavelength effects encountered in high field solid state NMR experiments makes it difficult to achieve uniform CP enhancement throughout the sample when the probe employs a single multiply tuned solenoidal coil. The use of a balancing element in the hf channel to symmetrize the hf RF field with respect to the coil is demonstrated here as one possible solution to this problem.

## Acknowledgments

This work was supported in part by the Wm. M. Keck foundation, Yale University, ExxonMobil Engineering and Research Corporation and a grant from the National Science Foundation. KWZ thanks Dr. Thomas Barbara for providing [14].

## References

[1] E.O. Stejskal, J. Schaefer, J.S. Waugh, Magic-angle spinning and polarization transfer in proton-enhanced NMR, J. Magn. Reson. 28 (1977) 105–112.
[2] X.L. Wu, K.W. Zilm, Cross-polarization with high-speed magic-angle-spinning, J. Magn. Reson. A 104 (1993) 154–165.
[3] Z.H. Gan, D.M. Grant, Rotational resonance in a spin-lock field for solid-state NMR, Chem. Phys. Lett. 168 (1990) 304–308.
[4] Y. Ishii, J. Ashida, T. Terao, C-13-H-1 Dipolar recoupling dynamics in C-13 multiple-pulse solid-state NMR, Chem. Phys. Lett. 246 (1995) 439–445.
[5] G.C. Campbell, L.G. Galya, A.J. Beeler, A.D. English, Effect of Rf inhomogeneity upon quantitative solid-state NMR measurements, J. Magn. Reson. A 112 (1995) 225–228.
[6] S. Idziak, U. Haeberlen, Design and construction of a high homogeneity RF coil for solid-state multiple-pulse NMR, J. Magn. Reson. 50 (1982) 281–288.
[7] A.F. Privalov, S.V. Dvinskikh, H.M. Vieth, Coil design for large-volume high-$B_1$ homogeneity for solid-state NMR applications, J. Magn. Reson. A 123 (1996) 157–160.
[8] F.H. Larsen, P. Daugaard, H.J. Jakobsen, N.C. Nielsen, Improving RF field homogeneity in solid-state MAS NMR using a loop-gap resonator, J. Magn. Reson. A 115 (1995) 283–286.
[9] F. Engelke, Electromagnetic wave compression and radio frequency homogeneity in NMR solenoidal coils: Computational approach, Concepts Magn. Reson. 15 (2002) 129–155.
[10] G. Metz, X.L. Wu, S.O. Smith, Ramped-amplitude cross-polarization in magic-angle-spinning NMR, J. Magn. Reson. A 110 (1994) 219–227.
[11] O. Stuhlman Jr., S. Githens Jr., The magnetic field of a solenoid oscillating at radio frequencies, Rev. Sci. Instrum. 3 (1932) 561–571.
[12] C.-N. Chen, D.I. Hoult, Biomedical Magnetic Resonance Technology, Adam Hilger, Bristol and New York, 1989, pp. 340.
[13] R.W. Martin, E.K. Paulson, K.W. Zilm, Design of a triple resonance magic angle sample spinning probe for high field solid state nuclear magnetic resonance, Rev. Sci. Instrum. 74 (2003) 3045–3061.
[14] E.L. Ginzton, Microwave Measurements, McGraw Hill, 1957, pp. 435–461.
[15] W.E. Maas, A. Bielecki, M. Ziliox, F.H. Laukien, D.G. Cory, Magnetic field gradients in solid state magic angle spinning NMR, J. Magn. Reson. 141 (1999) 29–33.
[16] F.D. Doty, G. Entzminger, Y.A. Yang, Magnetism in high-resolution NMR probe design. II: HR MAS, Concepts Magn. Reson. 10 (1998) 239–260.